Minerals Engineering 249 (2026) 110704

Contents lists available at ScienceDirect

Minerals Engineering

journal homepage: www.elsevier.com/locate/mineng

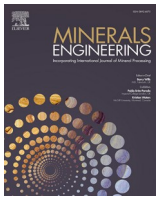

Advancing coarse particle flotation: how the NovaCell™ overcomes liberation challenges☆

Lonn M. Cooper [a,*], Graeme J. Jameson [b], Sherwin Morgan [c]

[a] Technical Expert – Flotation, Jord International Pty Limited, St Leonards, NSW 2065, Australia
[b] Emeritus Professor – School of Engineering, University of Newcastle, NSW 2308, Australia
[c] Technology Manager – NovaCell, Jord International Pty Limited, St Leonards, NSW 2065, Australia

ARTICLE INFO

Keywords:
Coarse particle flotation
Fluidized bed
Composite particles
Flotation
NovaCell™
Liberation
Detachment

ABSTRACT

For the successful recovery of coarse and composite particles by flotation, it is crucial to prevent or limit particle detachment. In conventional flotation machines, the strong hydrodynamic forces essential for bubble-particle collisions and attachment frequently lead to unintended detachment. The likelihood of detachment increases as particle size increases and as fractional surface liberation decreases. The NovaCell™ seeks to overcome this problem by using two distinct recovery zones that target coarse and fine particles separately, the former being achieved using a quiescent fluidized bed. Recent NovaCell™ studies have observed improved recovery efficiency at coarser grind sizes when compared to conventional flotation machines (Morgan et al., 2024). This is thought to result from decreased detachment of valuable particles with low surface liberation within the fluidized bed. Experiments were undertaken on a run-of-mine ore using the NovaCell™ and a mechanical cell. The NovaCell™ achieved greater copper recovery compared to the mechanical cell, especially at particle sizes above 100 μm. To explore this further, mineral liberation analysis was conducted on the NovaCell™ products. The flotation response for each size fraction and liberation class was determined, finding effective copper recovery across all size fractions with fractional surface liberation as low as 10 %.

1. Introduction

In response to the growing requirement to minimise emissions and water consumption in mineral processing, there is increasing research interest in strategies for the rejection of gangue minerals at coarser particle sizes (Batterham, 2013). Advantages of grinding to coarser particle sizes at the head of a flotation circuit are obvious and easily achievable in principle, including reduced energy and emissions per tonne of ore processed, increased throughput for existing equipment, easier water recovery, and improved tailings storage options. However, these benefits cannot be realised if the flotation process becomes the limiting factor. If coarse particles are unable to be recovered in the flotation circuit, major process efficiency loss will occur (Seaman and Vollert, 2017).

As particle size increases, a decline in flotation recovery is observed. This decline is well known and is attributed to a combination of reduced bubble-particle attachment efficiency and increased particle detachment. This detachment occurs both within the turbulent pulp phase driven by high-energy hydrodynamic forces and as preferential drop-back of coarse particles from the froth phase, all of which are influenced by the limiting interfacial chemistry between bubbles and particles (De F. Gontijo et al., 2007; Schulze, 1977). In a mechanical flotation cell, significant agitation is required to keep particles in suspension and disperse air bubbles throughout the pulp. The resultant turbulent flow fields facilitate high collision efficiency of bubbles and particles, leading to attachment and the formation of bubble-particle aggregates which can be recovered as a froth. However, the turbulence necessary for successful recovery of particles between 10 μm and 100 μm in a mechanical cell is detrimental to the flotation of coarse particles (Fuerstenau et al., 2007; King, 1982; Trahar, 1981). As particle size is increased beyond 100 μm, the turbulent conditions inside mechanical cells become deleterious as the relatively weak adhesion strength is dominated by increased drag and momentum of coarser particles, frequently leading to detachment as these particles are torn away from their bubble. The outcome is best demonstrated by Lynch et al. (1981) in the well-recognised “elephant curve” shown in Fig. 1 where it is clear

☆ This article is part of a special issue entitled: ‘Flotation?25′ published in Minerals Engineering.

* Corresponding author.
E-mail address: Lcooper@jord.com.au (L.M. Cooper).

https://doi.org/10.1016/j.mineng.2026.110704
Received 22 December 2025; Received in revised form 3 June 2026; Accepted 22 July 2026

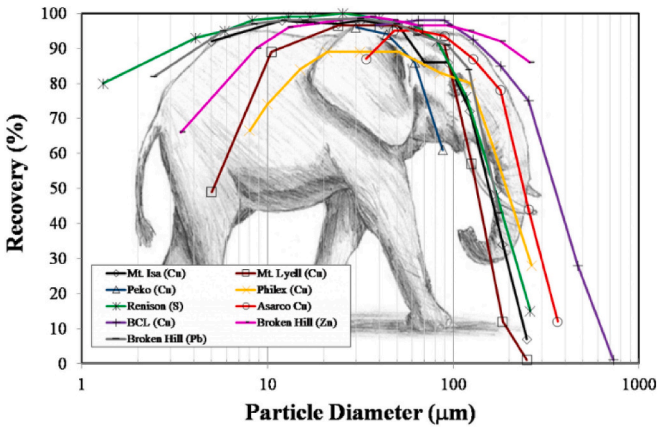

Fig. 1. Recovery by size flotation data for industrial sulfide flotation circuits (Lynch et al., 1981).

that flotation in conventional cells is only effective in a narrow particle size range.

To minimise detachment, it is ideal for coarse particle attachment to occur in an environment with minimal turbulence (Kohmuench et al., 2010; Soto and Barbery, 1991). It has been shown by Schulze (1984) that the maximum floatable particle size can increase to several millimetres when there is a more quiescent environment for flotation. The problem of increased detachment forces on coarse particles is compounded by the fact that as particle size increases, the fractional area of exposed hydrophobic sites typically decreases. This reduction in available attachment area reduces the adhesive force holding the particle to the bubble (Fosu et al., 2015b). Therefore, the challenge of floating coarse particles is twofold: the detachment forces are stronger, while the attachment forces are simultaneously weaker. It is clear that to increase flotation efficacy at coarser sizes, steps must be taken to reduce the exposure of bubble-particle aggregates to turbulence. One way of achieving this is through the use of a fluidized bed which aims to provide a quiescent environment where attachment of coarse particles can occur (Jameson, 2010; Kohmuench et al., 2001). One such flotation machine that utilises a fluidized bed is the NovaCell™, invented by Emeritus Professor Graeme Jameson. The NovaCell™ is a universal froth flotation machine, capable of recovering valuable minerals over a wide range of particle sizes. The design processes the feed sequentially to optimise recovery across a wide size range. Pulp first enters a pressurised pneumatic downcomer, which provides a shielded, high-intensity contacting region specifically for collecting fine particles. Following this intense aeration, the flow enters a quiescent fluidized bed which facilitates the attachment and recovery of coarse particles. Because the high-intensity environment is enclosed and strictly precedes the fluidized bed, coarse particles that attach in the quiescent zone are never exposed to the unwanted turbulence that would otherwise cause detachment.

A recent study at Pinto Valley Mine assessed NovaCell™ performance in coarse particle flotation circuits compared to conventional mechanical cells (Morgan et al., 2023). When replacing mechanical flotation cells, NovaCell™ demonstrated the potential to increase plant throughput by 20 % and reduce carbon emissions by 15 %. Further studies comparing the NovaCell™ to conventional mechanical cells have shown consistent performance benefits in the recovery of coarse particles (Morgan et al., 2024). The improved recovery in the NovaCell™ is a direct result of its reduced turbulence, which minimises the detachment forces that coarse bubble-particle aggregates are exposed to.

Muganda et al., (2011) showed that for fully liberated chalcopyrite in a laboratory mechanical cell, near-complete recovery was achieved for particles between 53 μm and 150 μm. However the recovery decreased as particle size increased above 150 μm. By contrast, Jameson and Emer (2024) showed that when using the more favourable hydrodynamic conditions of the NovaCell™, complete recovery of fully liberated chalcopyrite could be achieved at particle sizes up to at least 1400 μm. The effect on coarse particle recovery improvement in the NovaCell™ and other fluidized bed flotation cells is clear for fully liberated particles. However, it is suspected that the quiescent environment will also improve the recovery of poorly liberated particles which have much lower detachment forces. Fosu et al. (2015a) compared the recovery of synthetic composite particles between a mechanical cell and a different type of fluidized bed separator. They found a significant improvement in composite particle recovery in the fluidized bed separator, especially for particles with complex locking textures. In this paper, experiments were conducted in a laboratory NovaCell™ using a real ore to examine the recovery of composite particles by size and surface liberation, with a particular focus on very poorly liberated particles.

2. Experimental

2.1. Test methodology

A 100 kg run-of-mine (ROM) sample was collected from a concentrator plant located in Australia treating an iron oxide copper–gold (IOCG) ore body. The plant is currently operating with a flotation feed grind size P_{80} of 85 μm. The bulk sample was stage-crushed in a laboratory jaw crusher to a top size of 600 μm. The crusher product was homogenised and then split into 2 kg aliquots. A grindability study was conducted on the stage-crushed material using a laboratory rod mill to produce the required feed particle size distribution (PSD). Immediately prior to each flotation test, aliquots of the stage-crushed material were ground to the target size in the rod mill. Flotation tests were then performed in both the NovaCell™ and a mechanical cell (Agitair) which would serve as a performance benchmark for conventional flotation machines. Both tests were conducted with identical feed and reagent conditions. Crucially, the specific reagent suite (including the use of a short-chain xanthate collector) was strictly fixed by the ore supplier to mirror the current operating conditions of the plant. Due to project scope constraints that limited the capacity for full physical or chemical parameter optimisation, it was decided to conduct the comparative evaluation using this established industrial baseline.

A “flotation to extinction” test was conducted in each machine where the test was run until the froth appeared totally barren, followed by an additional 10-minute period. As the primary objective of this study was to isolate and quantify the recovery of poorly liberated material, this extended flotation to extinction approach was utilised specifically to eliminate kinetic constraints for slow-floating coarse particles, rather than to optimise froth stability or overall absolute recovery. Because the tests were designed exclusively to determine ultimate metallurgical recovery limits, a single cumulative concentrate sample was collected until the point of extinction, precluding the analysis of time-resolved mass or grade kinetics. Furthermore, collecting the concentrate as a single bulk sample was physically necessary to ensure that sufficient mass was available in the coarser size fractions for the subsequent size-by-size mineralogical analysis. A pair of 2 kg aliquots were individually ground with the same conditions as those used in the flotation tests for the purpose of feed characterisation. These feed samples, as well as all concentrate and tailings samples from each flotation test were dewatered, dried, weighed, wet screened, and then each size fraction was again dried and weighed. The screen sizes used were 212 μm, 106 μm, and 53 μm, creating 4 size fractions for analysis. Prior to pulverising, sub-samples from each size fraction of the feed, concentrate, and tails of the NovaCell test were taken and subjected to mineral liberation analysis (MLA). Ideally, products from the mechanical cell would also have undergone liberation analysis, however due to the cost constraints, priority was given to scanning a larger number of samples from the NovaCell™ to ensure statistical reliability. All remaining samples were then pulverised and assayed for elemental content using ICP-OES. The assay data was combined with the dry masses and a self-consistent mass balance was performed using the generalised least squares method to determine

the flotation performance for each test on a size-by-size basis. Subsamples of each size fraction sent for MLA were cast in resin, polished, and carbon coated prior to being scanned by electron microscope. The MLA XBSE method was used to provide quantitative mineral abundance and liberation data on a size-by-size basis. The MLA data obtained was reconciled with the balanced flotation data again using a generalised least squared error minimisation weighted against the confidence intervals of each measurement. This allowed for the determination of liberation of the flotation feed and calculation of liberation class recoveries. To establish experimental variance, the NovaCell™ flotation testing was performed in triplicate. While the mechanical cell evaluation consisted of a single test, the standard deviation derived from the NovaCell™ replicates was applied to the mechanical cell data. This approach assumes that the inherent methodological variance remained relatively constant across the experimental program. These calculated standard deviations are represented as error bars in the reported size-by-size recovery data. Because detailed MLA was performed on a specific representative test rather than a physical composite, the plotted error bars are anchored to the triplicate mean to accurately reflect variance. Additionally, where the applied variance exceeds physical boundaries (e.g., 0 % recovery), the error bounds have been truncated. The procedure is summarised in Fig. 2.

2.2. Feed properties

The particle size, copper distribution, and the copper grade of the feed used in both flotation tests is presented in Table 1. The P_{80} generated by the rod mill was 140 μm, considerably coarser than the plant's current flotation feed P_{80} of 85 μm. As is typical in many copper sulfide ores, the softer sulfide minerals tended to concentrate into the finer fractions as they were preferentially ground in the mill. Notably, the coarsest fraction (300–212 μm) containing 2.1 % of the mass only contained 1.1 % of the copper in the feed, placing a limitation on the overall obtainable benefit of recovering particles in this fraction. However, there was a much larger portion (23 %) of the total copper hosted in the 212–106 μm size fraction. It is important to note that the feed P_{80} of 140 μm used in this study was much finer than the feed used in previous NovaCell™ coarse particle flotation studies which have predominantly focussed on porphyry copper deposits (Morgan et al., 2024). This is due to the liberation characteristics of this IOCG ore body where the copper minerals are more finely disseminated and require a finer grind size to achieve comparable levels of liberation. Compositional information from the MLA data was used to produce a liberation spectrum following the approach of Wiegel (2006) by plotting the grade of particles containing each of the three identified copper sulfide minerals as a function of particle size as shown in Fig. 3. With interpretation described by Wightman & Evans (2014), extrapolation of the linear portion of the data shows that liberation of chalcopyrite begins at approximately 90 μm, while chalcocite and bornite begin to become liberated at 77 μm and 48 μm respectively. A feed P_{80} of 140 μm was chosen for the flotation tests, allowing for a suitable population of composite particles to evaluate the NovaCell™'s ability to recover poorly liberated particles.

To directly assess recovery performance under conditions of limited

Table 1
Feed mass and copper distribution and copper grade.

Particle size	Distribution		Grade
	Mass	Cu	Cu%
−300 + 212	2.1 %	1.1 %	1.22 %
−212 + 106	28.6 %	23.0 %	1.80 %
−106 + 53	23.0 %	22.9 %	2.23 %
−53	46.2 %	53.0 %	2.57 %
Total	100.0 %	100.0 %	2.25 %

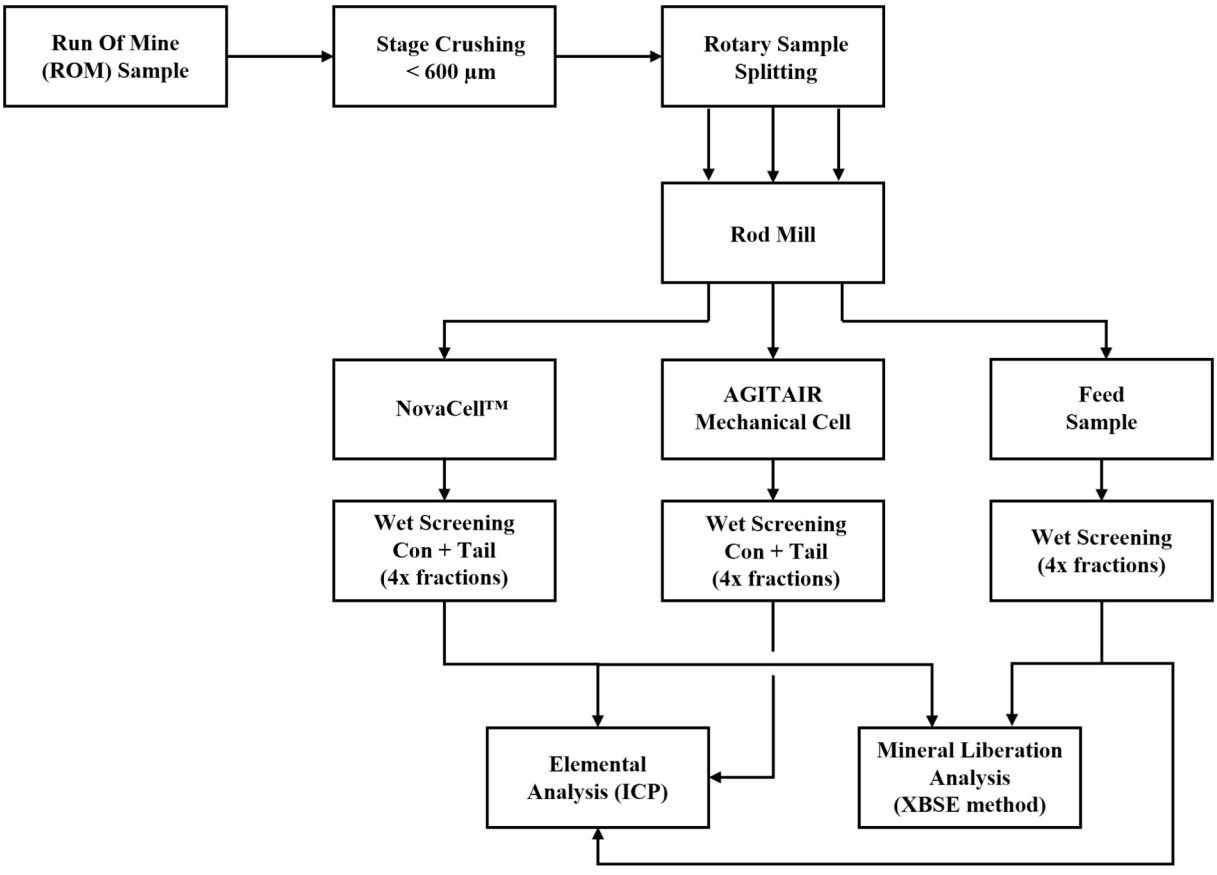

Fig. 2. Procedure for sample preparation and testing.

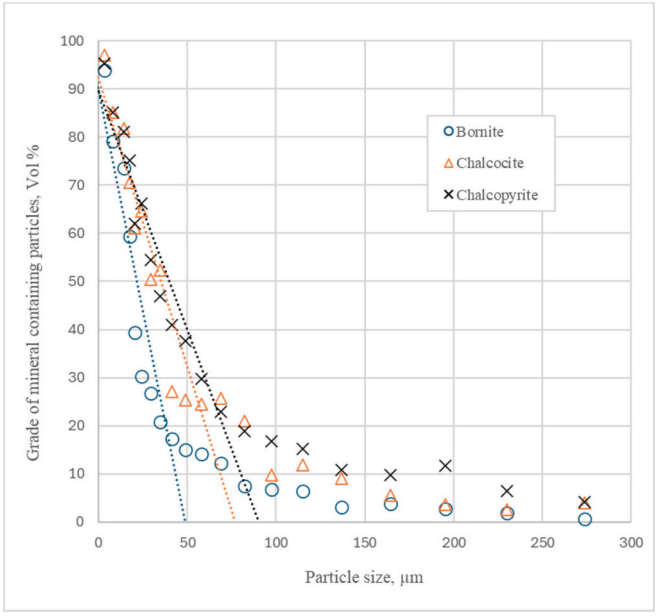

Fig. 3. Liberation spectrum of bornite, chalcocite, and chalcopyrite.

surface exposure, it was critical to decouple the effects of surface liberation from absolute particle size. Previous studies demonstrate that conventional mechanical cells experience a sharp drop in recovery for particles above roughly 150 µm purely due to hydrodynamic detachment, even when those particles are 100 % liberated (Muganda et al., 2011). By contrast, the NovaCell™ can achieve complete recovery of fully liberated particles up to at least 1400 µm (Jameson and Emer, 2024). If an ore that liberates at a much coarser size were evaluated, the mechanical cell would fail to recover them strictly because of their physical size, masking any liberation specific effects. The chosen IOCG ore avoids this confounding variable because it exhibits poor liberation at relatively fine sizes (100–300 µm) where mechanical cells are historically capable of recovering fully liberated particles, isolating surface liberation as the primary restrictive variable. This allows for a valid, direct comparison of how the differing hydrodynamics of the two machines influence the recovery of composite particles.

2.3. Flotation tests

2.3.1. Flotation in a mechanical cell

The mechanical cell test was run in an AGITAIR model LA-500 using a 5-litre cell with a 107 mm diameter impeller rotating at 500 RPM. A 2 kg aliquot from the rod mill was placed in the cell and topped up with water to a feed density of 30 % solids by weight. The pH of the pulp was measured to be 8.2 (natural, not adjusted) and then a collector, sodium ethyl xanthate (SEX) was added to the agitated cell at a concentration of 28 g/t and allowed to condition for 5 min. After conditioning, a frother (IF236N, a proprietary mixture of alcohols and glycol ethers) was added at a concentration of 25 ppm by volume. One minute after the frother was added, the air supply was turned on at 17 L per minute, corresponding to a superficial gas velocity (J_g) of 1.02 cm/s. A constant froth depth of 20 mm was maintained by topping up the cell with water containing frother throughout the test. Froth was recovered manually by scraping the entire surface of the cell every 10 s, with the concentrate collected via the overflow launder. After 5 min of flotation time, the froth appeared barren, and the air rate was increased to 20 L per minute. Concentrate was collected for an additional 10 min to allow for maximum recovery. Throughout the test, a total of 0.65 L of makeup water was added to maintain the froth depth.

2.3.2. Flotation in NovaCell™

To complete a NovaCell™ test, five 2 kg aliquots were individually ground in the rod mill and then combined with water to produce a 10 kg feed of 30 % solids by weight. The difference in feed mass between the mechanical cell test and NovaCell™ test is due to the minimum operating volume of each system. Specifically, while the mechanical cell operates with a 5-litre volume, the laboratory NovaCell™ circuit requires a minimum operating volume of 25 L. The pulp was then added to the laboratory NovaCell™ system shown in Fig. 4. The Downcomer pump recirculates the pulp by pumping it from the Recycle/Feed sump to the downcomer which injects the flow into the base of the flotation column. Pulp exiting the downcomer flows upward and into a collection cone where it gravitates through a vibrating screen (in this test using a sieve aperture of 180 µm) and back to the Recycle/Feed sump.

In the absence of reagents and air, the NovaCell acts as an elutriator. It was found that when using a sieve aperture of 180 µm, no coarse particles, whether gangue or chalcopyrite, were recovered on the vibrating screen. This observation confirmed that if coarse particles were found on the screen during flotation runs, they could only have reached the collection cone by attachment to bubbles. Under the chosen superficial liquid velocity, the coarse gangue particles, being non-hydrophobic, never reached the top of the column. The screen underflow, which contained particles less than 180 µm in diameter, flowed back to the feed tank as the recycle stream.

With the pulp circulating in a closed loop, collector (SEX) was added to the sump and allowed to circulate for 5 min before frother (IF236N) was added to the system. Collector and frother concentrations were the same as in the mechanical test: 28 g/t and 25 ppm respectively. 1 min after the frother was added, a metered supply of compressed air was supplied to the downcomer at a rate of 4.6 L per minute to provide the same J_g (1.02 cm/s) as in the mechanical cell test. For both machines, J_g was calculated using total cross-sectional area. Because both cells feature straight, parallel walls in their active separation zones, the cross-sectional area is constant and J_g remains uniform throughout the vertical profile of each unit. Furthermore, because material continuously circulates from the external sump into the active reactor zone during the NovaCell™ batch tests, the instantaneous transport load to the froth is distributed over the duration of the test. This fundamental batch artifact prevents direct carrying capacity or instantaneous transport load comparisons with the mechanical cell, where 100 % of the feed mass is simultaneously aerated.

As air mixed with the recycle flow, turbulent mixing and attachment of fine particles occurred within the downcomer. Since finer particles can withstand higher detachment forces, they remain attached as they

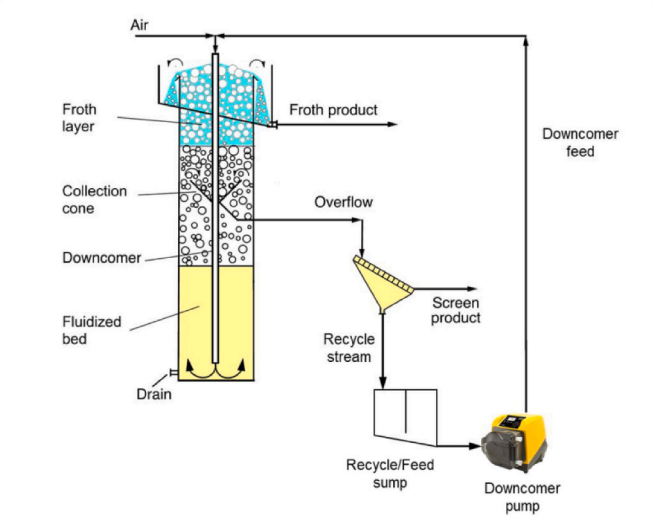

Fig. 4. Schematic of NovaCell™ batch test.

are injected at the base of the cell. Bubbles then flowed upward through the fluidized bed where high rates of collision occur with coarse particles, causing them to attach and rise with the bubbles. Bubbles loaded with fine and coarse particles float to the top of the column, maintaining a froth depth of 110 mm. The froth layer flowed continuously over the lip into an overflow launder, where it was collected as concentrate without the need for manual scraping or makeup water. Some coarse particles may become detached from their bubble either from within the froth or upon impact with the froth interface; this is known as "drop-back" (Ata, 2012; Falutsu and Dobby, 1989; Finch and Dobby, 1990). It is also possible that some coarse particles attached to bubbles do not enter the froth because the bubble-particle aggregates are too dense to pass through the interface, as the froth apparent density is much lower than that of the underlying pulp layer (Jameson and Emer, 2024). This limitation is compounded by the fluid dynamics above the collection cone. Because the majority of the circulating pulp required for fluidization exits through the cone, the upward fluid velocity drops significantly in the region above it. Consequently, some bubble-particle aggregates with high apparent densities, which were only able to rise due to the strong upward drag in the fluidized bed, lose this supporting flow in the calmer upper zone and begin to sink. The collection cone is designed to capture these sinking aggregates, as well as any particles that detach above the cone, using opposing fluid velocities at the cone entry; a strong upward flow in the outer annulus prevents particles from falling back into the fluidized bed, while a rapid downward flow actively pulls them into the cone. Since these particles are too coarse to reach the collection cone by elutriation alone, they must only be present due to buoyancy modification by attachment to a bubble, thus they have some component of hydrophobicity and are therefore considered to be valuable. These particles are too coarse to pass the vibrating screen and are captured on top while the remaining liquid and fines pass through. The material captured on the screen is treated as a second concentrate stream, aiding the NovaCell™ in recovering drop-back particles and particles that would be difficult to recover in the froth phase due to the critical buoyancy limitation. While this screen capture mechanism is highly effective for coarse particles, the froth zone remains essential for the selective recovery of fine particles. The pulp passing through the screen is sent back to the agitated Recycle/Feed sump where it mixes with feed material and is pumped again to the downcomer. For the duration of the test, single cumulative concentrate samples were collected from both the froth launder and the screen. As in the mechanical cell test, after approximately 6 min, the froth became barren although coarse particles were still observed to be flowing into the froth launder in the absence of significant fine material. The test was allowed to progress to a total of 16 min. The material remaining in the system (including the NovaCell™, the feed/recycle sump, and all pipework) was flushed out via a drain valve at the base of the cell (which remained closed during the active flotation period) and collected, becoming the tailings sample for the test.

2.4. MLA data handling

All references to liberation in this study refer to 2D surface exposure measured via MLA. Analysis of the raw MLA data revealed many particles with equivalent circle diameters (ECD) significantly smaller than their respective sieve fractions. This is a recognised stereological artifact inherent to 2D imaging. When a coarse composite particle is sectioned, it can produce an artificially small 2D fragment. When this occurs, only a small peak or corner of a much larger 3D composite particle is scanned and is misreported as highly liberated or completely barren, compounding stereological bias and skewing the true liberation distribution. To account for standard stereological biases where 2D sectioning typically overestimates true 3D liberation (Miller et al., 2009), a filtering protocol was applied. Particles with an equivalent circle diameter below 25 % of the sieve aperture used to prepare the sample were excluded from the three coarsest size fractions. The 53–0 μm fraction remained unfiltered.

Statistical reliability for each liberation class was established by calculating 95 % confidence limits based on particle counts (Leigh et al., 1993). To minimise variance propagation from sparsely populated intermediate classes (Deming, 1938), liberation intervals were consolidated into statistically robust groups. To maintain high resolution for the poorly liberated composite particles central to this study, the 0–40 % range was analysed in 10 % increments. The remaining classes were grouped as 40–<70 %, 70–<100 %, and fully liberated. The resultant particle counts for these condensed intervals are shown in Fig. 5.

3. Results and discussion

3.1. Mineralogical characterisation

A representative sample of each size fraction of the feed was scanned by electron microscope. In total, 216,548 particles were scanned, with 15,819 particles found to contain a copper sulfide mineral. After filtering, 591 of the copper sulfide containing particles were rejected using the exclusion criteria with 15,228 particles being used in the analysis. The copper sulfide minerals present in the feed were almost exclusively bornite, chalcocite and chalcopyrite. Some trace amounts of carrolite and covellite were found, however they were negligible. No native copper or copper oxide minerals were found in the scanned samples which simplified the reconciliation with copper assays produced using ICP-OES. Table 2 shows how the copper in the feed was distributed within each of these minerals as well as the distribution of mass of each mineral within the total of observed copper sulfide minerals. Since chalcocite was the lowest contributor to the total copper content and it also contains the highest proportion of copper by mineral weight, the mineral mass distribution was significantly lower compared to the chalcopyrite. 16.0 % of the total copper was hosted in chalcocite, while only 5.9 % of the copper sulfide mineral mass was from chalcocite. By contrast, 53.7 % of the copper was hosted in chalcopyrite which made up 72.3 % of the copper sulfide mineral mass. Table 3 shows the mineral grain size passing diameters for the three major minerals and the sum of all copper sulfide minerals. In this case, the grain size is being taken as the equivalent circle diameter, which is the diameter of a circle which has the same area as the grain being analysed. It is clear that the chalcopyrite native grain size was larger than that of either bornite or chalcocite grains.

The large difference in mineral mass combined with the finer grain size distribution of chalcocite and bornite resulted in fewer individual particles found in each liberation class of the coarse size fractions, ultimately increasing the confidence interval for these minerals when compared to chalcopyrite. Bornite was also affected, but to a lesser extent. Figs. 6, 7, and 8 show a comparison of the confidence limits for each liberation class of each mineral for the 212–106 μm size fraction of the feed.

As the particle size increases relative to the grain size, it is expected that the distribution of copper minerals into the poorly liberated size classes will also increase. This is confirmed in Fig. 9 which illustrates a clear shift in copper distribution across the measured size fractions. For the finest fraction, the copper distribution is heavily skewed toward complete liberation. As particle size increases, the distribution flattens, and for the coarsest fractions, the trend reverses, with most of the copper distributed in particles occupying the lowest surface liberation classes. Comparing opposite ends of the spectrum, 74 % of the copper in the −53 μm fraction was 100 % liberated while only 4 % had a surface liberation of less than 30 %. By contrast, only 3 % of the copper in the 300–212 μm fraction was 100 % liberated while 71 % had a surface liberation less than 30 %. The deportment of copper minerals into each surface liberation class is shown in Fig. 10 where almost half (48.6 %) of the total copper in the feed was completely liberated while only 1.3 % of the feed copper had no surface liberation at all. For the purposes of this study, 18 % of the total copper was hosted in the liberation classes between 0 %

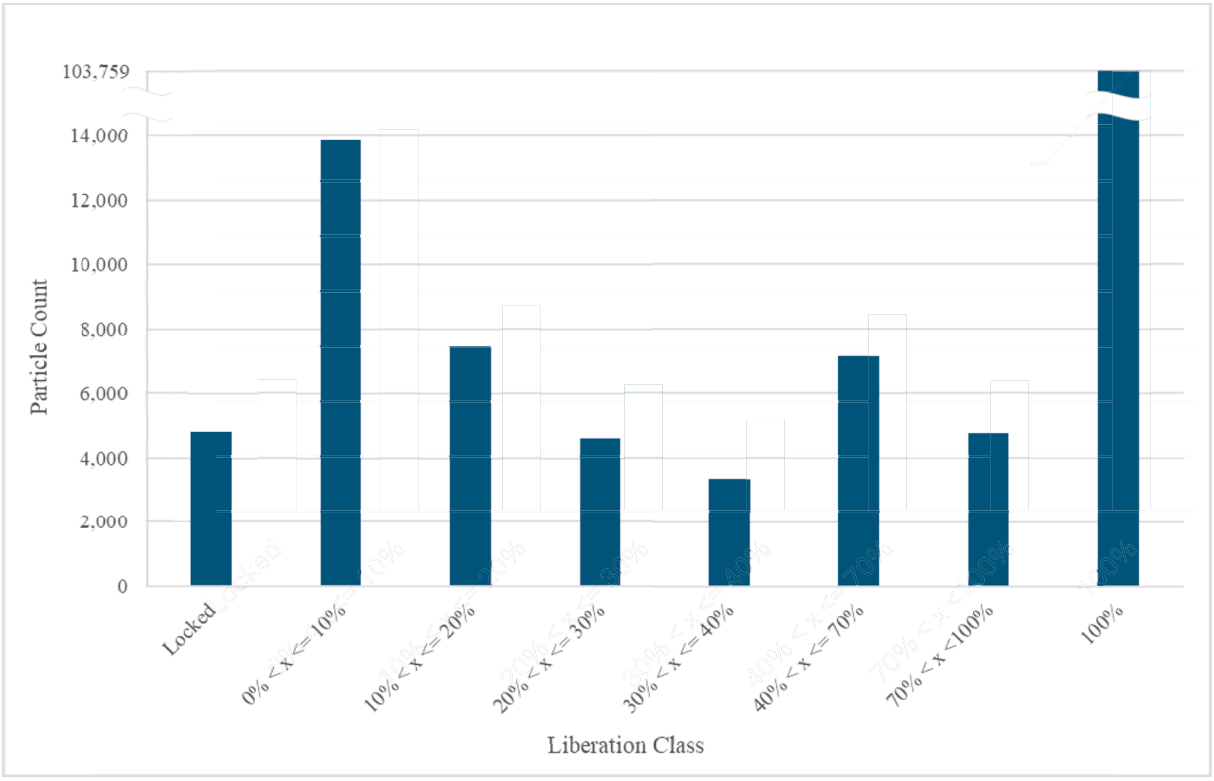

Fig. 5. Number of particles identified containing a copper sulfide mineral in each liberation class after combining sparsely populated classes. Note that the Y axis has been limited to allow readability.

Table 2
Copper distribution within sulfide minerals and mineral distribution within copper sulfide minerals.

Particle size	Elemental Distribution (Cu)			Mineral Distribution (%Wt)		
	Bornite	Chalcocite	Chalcopyrite	Bornite	Chalcocite	Chalcopyrite
−300 + 212	33.0 %	23.7 %	43.3 %	25.1 %	14.3 %	60.5 %
−212 + 106	30.3 %	23.4 %	46.3 %	23.9 %	9.3 %	66.8 %
−106 + 53	31.4 %	24.2 %	44.4 %	25.1 %	9.8 %	65.1 %
−53	30.1 %	15.8 %	54.1 %	21.9 %	5.8 %	72.3 %
Total	29.6 %	16.0 %	53.7 %	21.7 %	5.9 %	72.3 %

Table 3
Mineral grain size passing diameters (μm equivalent circle).

% Passing	Bornite	Chalcocite	Chalcopyrite	Total Cu Sulfides
90	98.1	168.0	187.6	177.5
80	78.6	156.0	165.3	153.5
50	35.7	55.1	90.8	74.6
20	15.4	21.7	38.3	30.2
10	9.8	13.8	23.6	17.8

and 30 % which is generally considered to be so poorly liberated and difficult to recover by flotation that they are often grouped together and treated as “locked” (Lotter et al., 2018, Lotter et al. (2002)). It should be noted that in evaluating this copper deportment and subsequent recovery, all identified copper sulfide minerals have been grouped together. While these minerals naturally possess different inherent floatability, analysing recovery on an individual mineral basis resulted in sparsely populated data sets with unacceptably wide confidence intervals. Therefore, grouping them was a necessary statistical trade-off to ensure robust recovery calculations, operating under the assumption of equal floatability for the overall liberation analysis.

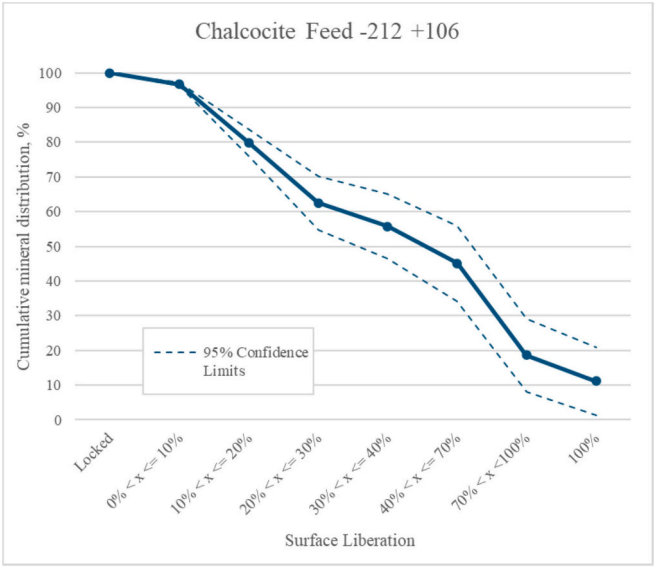

Fig. 6. Confidence limits for chalcocite in the 212–106 μm fraction of the feed.

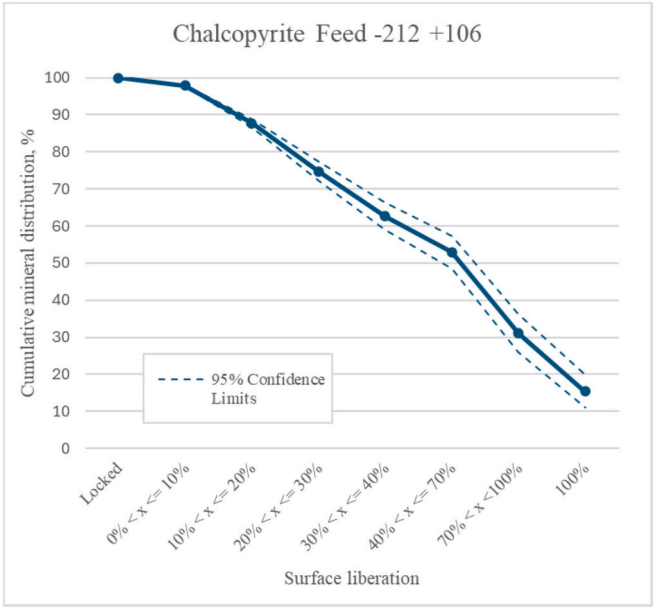

Fig. 7. Confidence limits for chalcopyrite in the 212–106 μm fraction of the feed.

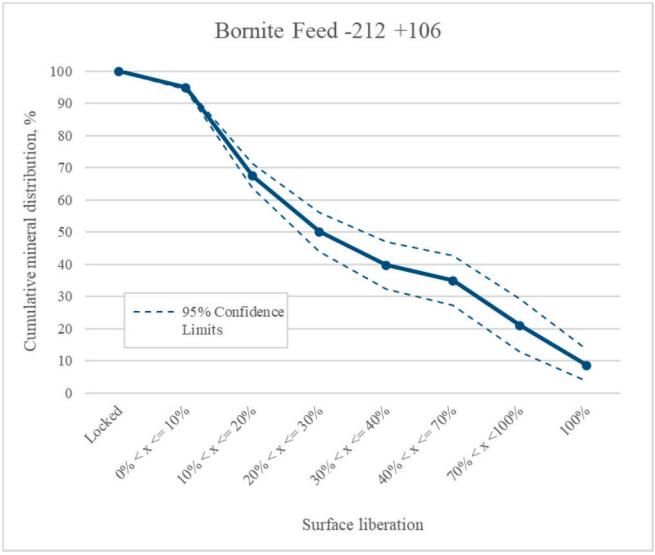

Fig. 8. Confidence limits for bornite in the 212–106 μm fraction of the feed.

3.2. Flotation recovery data

The overall and size-by-size copper recovery obtained in both the mechanically agitated cell and the NovaCell™ is presented in Fig. 11. The overall copper recovery obtained from the mechanical cell was 89.4 % ± 0.8 %. The size-by-size recovery data shows that as particle size increases above 106 μm, there is a sharp decrease in recovery for the mechanical cell, with no particles larger than 212 μm being found in the concentrate. When flotation took place in the NovaCell™, the overall recovery increased to 94.3 % ± 0.8 %. This higher overall recovery can be attributed to a significant improvement in recovery of coarse particles, with the difference between the NovaCell™ and the mechanical cell increasing as particle size increased. The recovery for the −53 μm fraction was comparable for both machines, within experimental error.

3.3. Size-by-size selectivity

To ensure that the enhanced coarse particle recoveries observed in the NovaCell™ were the result of genuine metallurgical selectivity rather than indiscriminate mass pull, the final mass yield, copper recovery, and concentrate grade for each size fraction were compared (Table 4). In batch flotation, an artificial increase in valuable recovery driven by non-selective mass pull (gangue entrainment) is universally accompanied by a severe decline in concentrate grade. However, Table 4 demonstrates that the NovaCell™ achieved superior coarse particle recovery without suffering the severe grade penalty associated with such entrainment. For example, in the −212 + 106 μm fraction, the NovaCell™ achieved a substantially higher copper recovery (91.8 %) than the mechanical cell (73.9 %), doing so with a mass pull of 22.4 % and a resulting concentrate grade of 7.4 % Cu. While this grade is naturally lower than that of fully liberated finer fractions, this is a physical inevitability of coarse particle flotation; successfully recovering poorly liberated composite particles inherently dictates that the physically attached gangue must also report to the concentrate. Despite this intrinsic limitation, the ability of the NovaCell™ to reject over 77 % of the total mass in this fraction confirms that its quiescent environment and screen-capture mechanism specifically target true hydrophobic bubble-particle aggregates, successfully rejecting fully liberated barren gangue rather than relying on indiscriminate mass recovery.

3.4. Overall recovery by liberation

In addition to the feed sample, samples of each size fraction of the concentrate and tailings from the NovaCell™ were also sent for liberation analysis. A total of 200,536 and 188,243 particles were scanned for the concentrate and tailings respectively. The scan located 75,065 copper sulfide-bearing particles in the concentrate and 3595 in the tailings. The fragment filter excluded 1949 particles from the concentrate and 53 from the tailings, with the remaining 73,116 concentrate and 3542 tailings particles being included in the analysis.

Fig. 12 shows the overall copper deportment for the feed, concentrate, and tails of the NovaCell™ test. Inspection of the losses to the tailings shows that almost all of the unrecovered copper is in the classes with <10 % liberation and the 100 % liberated class. The overall copper recovery for each liberation class is summarised in Table 5.

3.5. Size-by-size recovery by liberation

The copper recovery for each liberation class in each size fraction is presented in Fig. 13. While the data generally shows a sharp reduction in recovery below 10 % liberation, an anomaly exists for the 100 % liberated material. The losses from this class, originally identified in the overall tailings deportment (Fig. 12), are shown here to originate entirely from the −53 μm fraction, with all other size fractions having 100 % recovery. Fig. 14 confirms these losses are dominated by ultra-fine particles, with 60 % of the lost copper hosted in particles smaller than 5 μm. While high liberation is generally beneficial, this advantage is negated for ultra-fine particles, which have poor floatability regardless of their surface composition due to low collision efficiency for small particles with low inertia that are dominated by hydrodynamic drag forces (Miettinen et al., 2010). For the sake of contrast, the largest fully liberated particle in the upper left corner of Fig. 14 has an ECD of 40.0 μm and the next largest particle was 16.5 μm with the size decreasing monotonically. Of the 899 fully liberated particles identified, only 4 were larger than 10 μm. 60 % of the copper losses in the fully liberated class of the −53 μm fraction were hosted in particles smaller than 5 μm while only 20 % of the copper found in the same class and fraction of the feed were below 5 μm.

Additionally, Fig. 13 also shows little difference in recovery between the completely locked and 0–10 % liberation classes in the −53 μm fraction. This may be a result of stereological bias, where particles

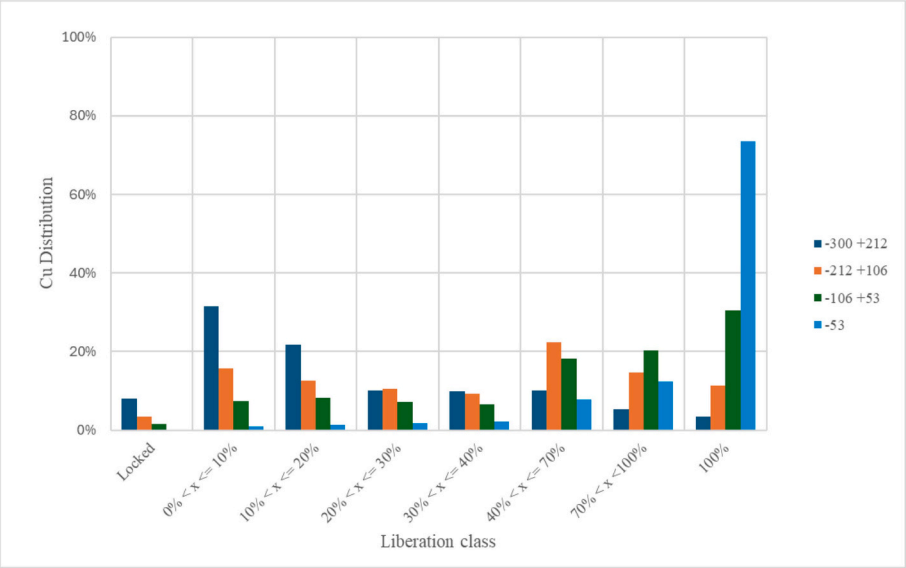

Fig. 9. Copper distribution by liberation class for each size fraction of the feed.

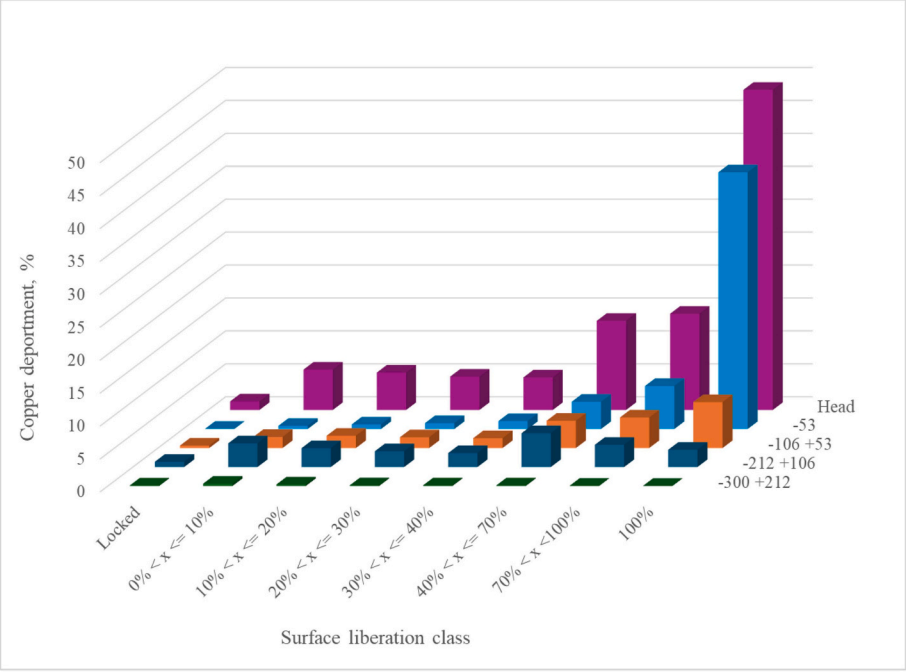

Fig. 10. Deportment of copper in feed by size and liberation class.

appear as fully locked despite having surface exposure that is not visible in the scanned section. This could also be due to "critical patch" size phenomenon. Assuming spherical scaling, the area of a hydrophobic site on a 20 μm particle is significantly smaller than the same fractional site on a 250 μm particle. A hydrophobic site on a fine composite particle may simply be too small to overcome the thermodynamic energy barrier required to rupture the water film, causing it to behave as though fully locked. A false colour image of the 0–10 % liberation class of the −53 μm fraction of the concentrate is shown in Fig. 15, providing a visual indication of the amount of surface exposure required for particle capture by bubbles.

To fully explore the impact of each size fraction and liberation class to overall copper recovery, the copper deportment of the concentrate and tailings is shown in Fig. 16. Here we can distribute the total 5.68 % of unrecovered feed copper lost to the tailings into four broad groups relating to their mechanism of loss:

1) 32 % (1.82 % absolute) was contained in the fully liberated −53 um fraction, mostly in the form of ultra-fines as already discussed.
2) 12 % (0.69 % absolute) was fully encapsulated in the locked liberation class with no measured surface exposure, making recovery by a surface chemistry process impossible.
3) 26 % (1.45 % absolute) was spread throughout all size fractions with more than 10 % surface liberation (excluding the −53um fraction with 100 % liberation).
4) The remaining 30 % (1.72 % absolute) was found in size fractions with less than 10 % liberation.

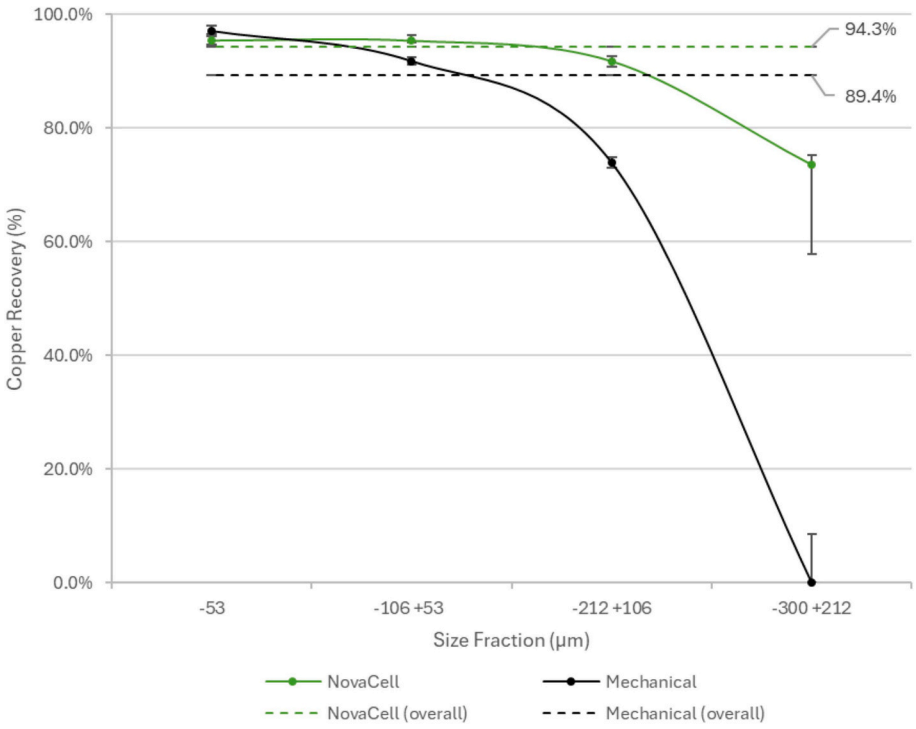

Fig. 11. Size-by-size copper recovery for the NovaCell™ and mechanical cell tests. Plotted points represent the specific NovaCell™ test subjected to MLA. Error bars represent ± 1 standard deviation derived from triplicate testing (see Section 2.1 for variance methodology).

Table 4
Size-by-size mass pull, copper recovery, and copper grade for the NovaCell™ and mechanical cell tests.

Particle size	Mass Rec (%)		Cu Rec (%)		Cu Grade (%)	
	NovaCell™	Agitair	NovaCell™	Agitair	NovaCell™	Agitair
−300 + 212	16.3 %	0.0 %	73.6 %	0.0 %	5.5 %	–
−212 + 106	22.4 %	10.5 %	91.8 %	73.9 %	7.4 %	12.7 %
−106 + 53	15.0 %	11.3 %	95.4 %	91.8 %	14.2 %	18.2 %
−53	12.1 %	10.1 %	95.4 %	97.1 %	20.3 %	24.7 %
Sum	15.8 %	10.2 %	94.3 %	89.4 %	13.4 %	19.6 %

Reviewing the confidence limit plots for the tailings (Fig. 17), it can be seen that the confidence intervals are wider for coarser fractions and for particles with greater than 10 % liberation due to the lower particle counts. However, this uncertainty primarily affects classification within the same broad group (e.g., a particle shifting between the 40–70 % and 30–40 % liberation classes). The probability of a particle crossing the boundary between major groups, for example, a particle with <10 % liberation being misclassified as >10 % is statistically low. This supports the statistical validity of the four loss categories. An analysis of the cumulative distribution confirms that these measurement variances do not significantly alter the overall deportment of copper among the four defined loss groups.

3.6. *Proposed hydrodynamic size limit for poorly liberated coarse particles*

High recoveries of particles with more than 10 % surface liberation regardless of particle size, have been observed in other fluidized bed flotation studies (Mehrfert, 2017). Jameson (2012) examined flotation data from Welsby et al. (2010) using particles up to 100 µm and found that partial surface liberation affects the rate constants of all particles in the same way, independently of size. He then concluded that the decline in recovery of coarse particles has nothing to do with liberation and is only related to the hydrodynamic conditions in the flotation cell. This appears to be consistent with the data presented in Fig. 13 where all particle sizes experienced a sharp reduction in recovery at the same fractional surface liberation of below 10 %.

Fosu et al. (2015b) found that recovery of composite particles was significantly increased when using a fluidized bed separator when compared to a mechanical cell. Since the products from the mechanical cell in this study were not analysed for liberation, it is uncertain if the trend observed in Fig. 13 would be the same for the mechanical cell or if the liberation class where recovery sharply reduces occurs at a higher value of surface liberation for coarser particles.

In this study, the rate constants for flotation were not measured but rather the maximum recovery at pseudo-infinite time. Where the recovery of particles with at least partial surface liberation does not approach 100 %, we can infer that either those particles were extremely slow floating and that they were not able to be recovered in the time allowed, or that they were unable to be recovered regardless of the time allowed.

Further work should explore whether the observation of Jameson (2012) extends to size fractions coarser than 100 µm. It is possible that as particle size increases, there is a point where liberation becomes the limiting factor for the hydrodynamic environment characteristic of the flotation machine being used. For example, where hydrodynamic conditions are highly turbulent, poorly liberated coarse particles may be completely unrecoverable unless they have some minimum fractional liberation which provides an attachment force strong enough to avoid instant detachment. In a calmer environment, the detachment forces are

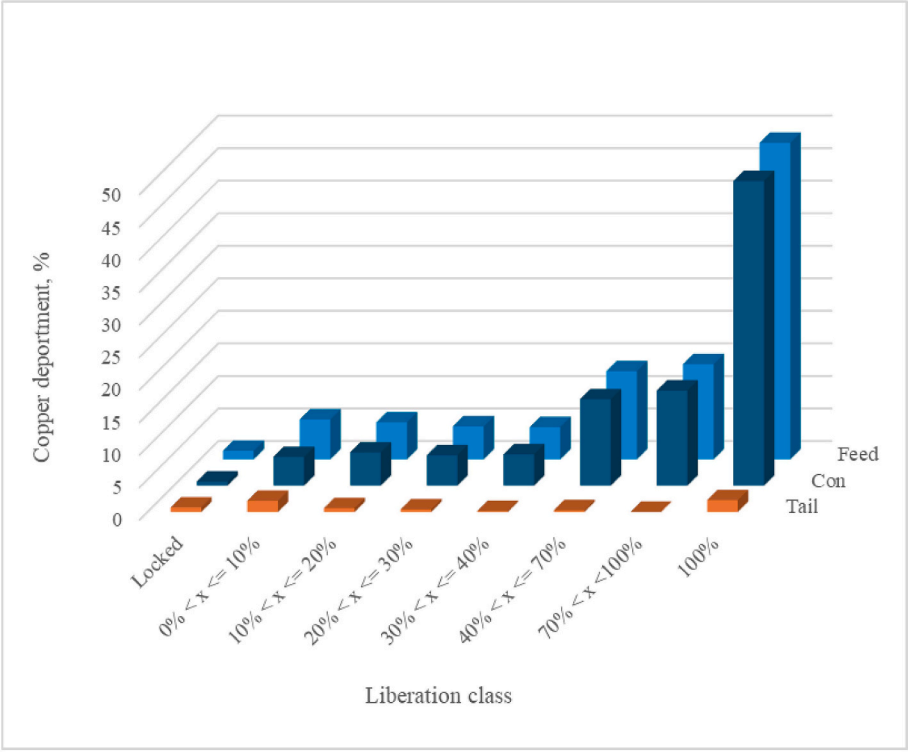

Fig. 12. Overall copper deportment for each liberation class into each stream of the NovaCell test.

Table 5
Overall copper recovery for each liberation class.

Liberation class	Locked	0 % < x <= 10 %	10 % < x <= 20 %	20 % < x <= 30 %	30 % < x <= 40 %	40 % < x <= 70 %	70 % < x < 100 %	100 %
Cu Recovery	47.4 %	71.9 %	89.6 %	92.1 %	97.0 %	98.0 %	99.9 %	96.3 %

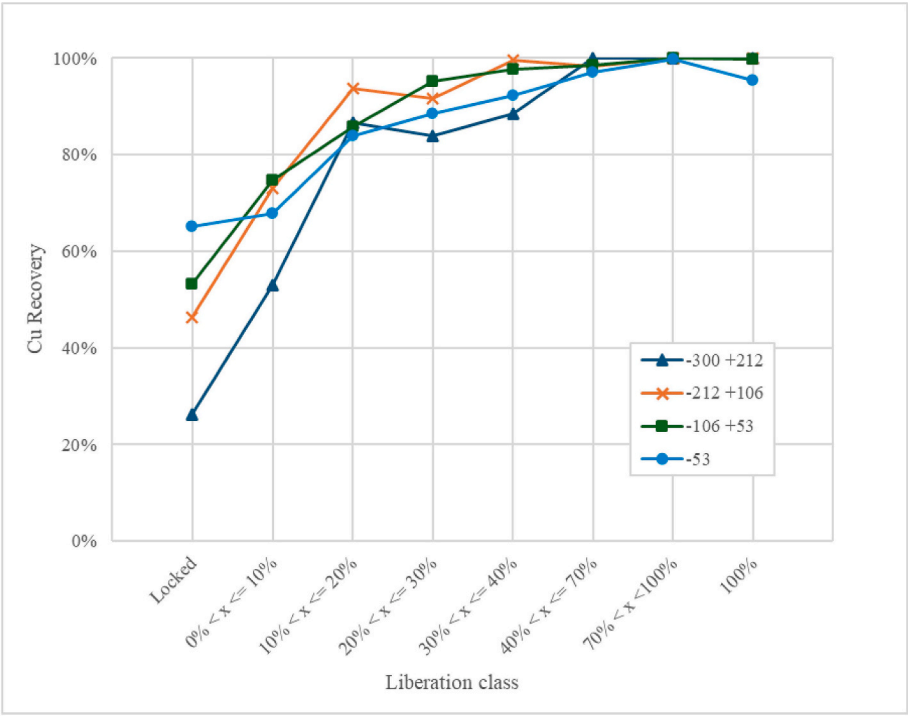

Fig. 13. Copper recovery for each liberation class of each size fraction for the NovaCell™ test.

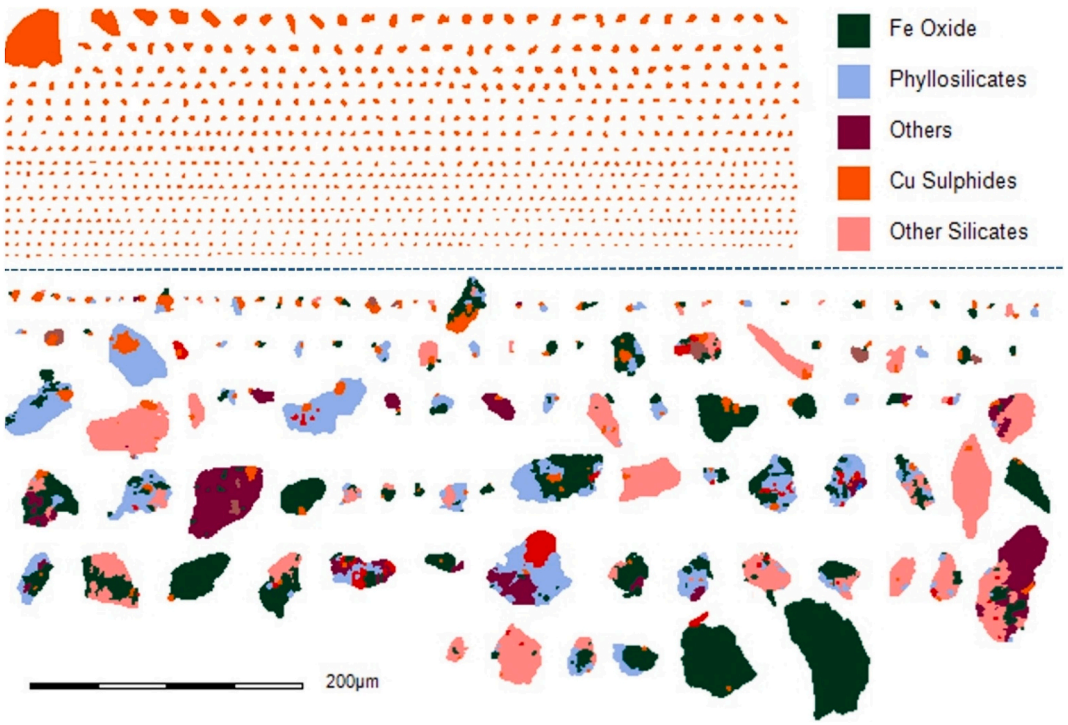

Fig. 14. False-colour image showing particles from the −53 µm fraction of the tailings sample. Particles above the dashed line are 100 % liberated and account for 79.4 % of the copper found in the −53 µm sample.

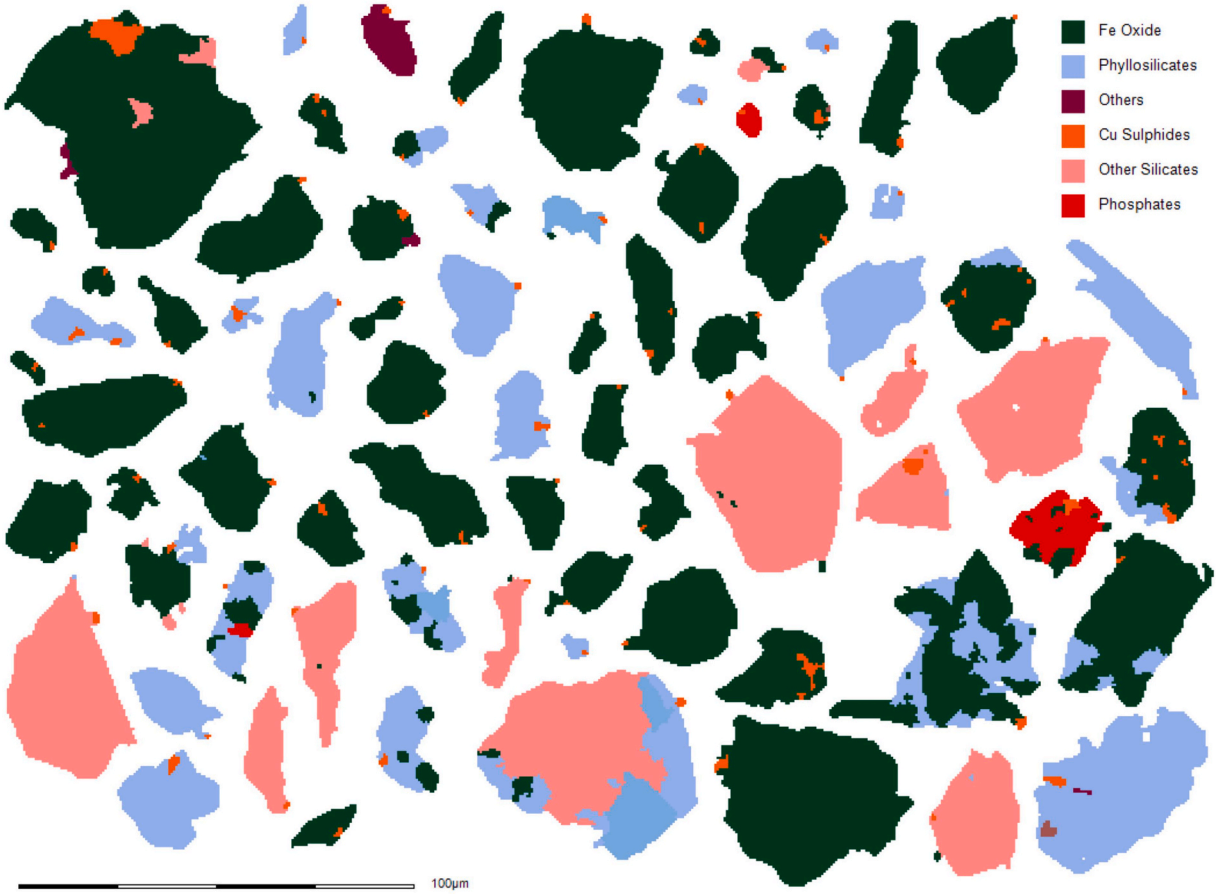

Fig. 15. False-colour image showing particles from the >0–10 % liberation class of the −53 µm fraction of the concentrate sample.

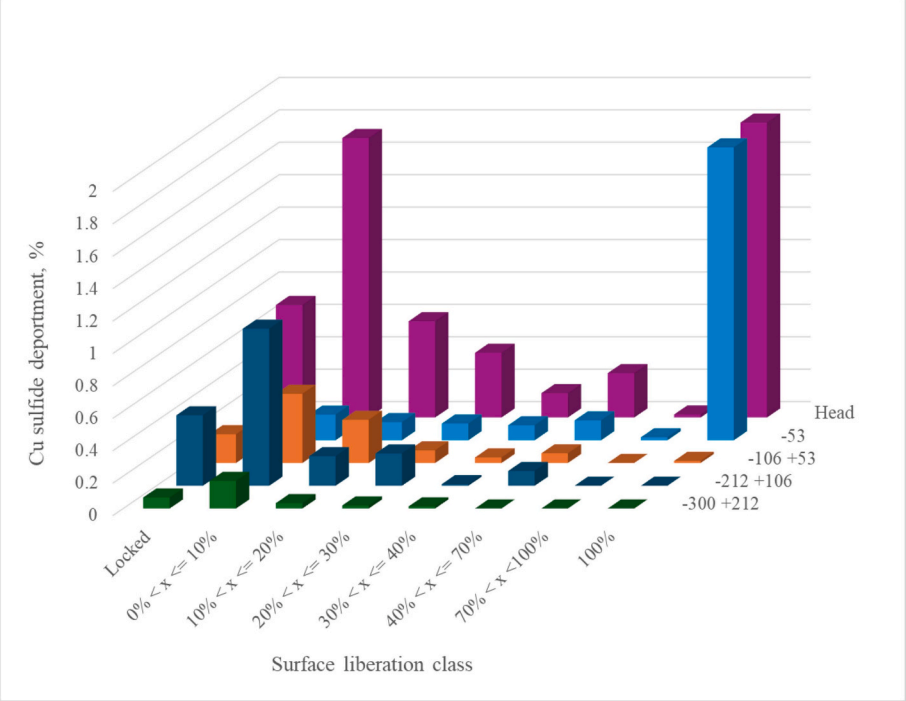

Fig. 16. Copper deportment of each size fraction and liberation class for the tailings stream.

much lower, so the extent of liberation required will likely be reduced. As particle size increases, the detachment forces are increased and the minimum surface liberation required to provide an attachment bond strong enough to avoid instant detachment will also increase. In this case, we could propose a modification to the "liberation function" proposed by Jameson (2012), which was found by relating the rate constant of a partially liberated particle to the rate constant for fully liberated particles at the same particle size. The modification would introduce a constraint whereby at some lower limit of liberation for particles above a certain size, the rate of flotation essentially becomes zero as these particles experience guaranteed detachment. We can see from Fig. 13 that as particle size increases beyond 212 μm, the reduction in recovery for the 0–10 % liberation class becomes more significant. Since the NovaCell™ is capable of ~100 % recovery of fully liberated particles as large as 1400 μm (Jameson and Emer, 2024), there must exist a particle size where 100 % of the fully liberated particles are recovered but no particles are recovered within the liberation class of 0–10 %.

3.7. Proposed mechanisms for enhanced recovery of composite particles

Analysis of the particles lost to tailings revealed a mixture of simple and complex locking textures. Fig. 18 shows false-colour particle images of particles with between 10 % and <100 % liberation found in the 212–106 μm and 106–53 μm size fractions of the tailings. Work by Fosu et al. (2015a) investigated textural effects on floatability in fluidized-bed separators compared to mechanically agitated flotation machines. They demonstrated that while fluidized-bed separators provide a marginal benefit for composite particles with simple locking textures, the benefit was significantly greater when recovering particles with complex locking textures, which are poorly recovered by mechanical cells. The superior performance of the NovaCell™ in the present study is therefore consistent with these findings, and its advantage can likely be attributed to the enhanced recovery of these complex-textured particles that were unlikely to be recovered by the mechanical cell.

Mechanisms for the recovery of particles with complex textures in a quiescent fluidized bed could be numerous. Simple locking textures usually provide a single relatively large hydrophobic attachment site, while complex textures will often have multiple but smaller hydrophobic sites. The shape of the particle and the hydrophobic attachment site have a large impact on the attachment force. Many investigations have shown that irregularly shaped particles and particles with rough surfaces exhibit higher forces of attachment and flotation rate when compared with rounder and smoother particles which experience higher detachment probability (Ahmed, 2010; Anfruns and Kitchener, 1976; Koh et al., 2009; Verrelli et al., 2014; Wotruba et al., 1991; Yekeler et al., 2004).

Gautam and Jameson (2012) showed that pinning of the three-phase contact line between a bubble and a particle occurred at sharp edges and corners of hydrophobic sites. Thus, the capillary force of attachment is increased for irregularly shaped sites when compared to a spherical particle of same wetted perimeter and contact angle. Additionally, where a single bubble bridges two closely adjacent attachment sites, an asymmetrical meniscus is formed as shown in Fig. 19, potentially influencing the contact angle and attachment force dependent on the separation distance between sites.

Generalising, for two particles of equal size and equal surface liberation, the textural distribution of those hydrophobic sites significantly impacts both collision efficiency and attachment force. A particle with a complex texture possesses multiple, smaller attachment sites distributed across its surface, which naturally provides a higher collision efficiency than a simple texture with a single, localised site. Crucially, these distributed sites are likely to exhibit a higher combined attachment force due to the contact line pinning and meniscus bridging effects described above. As a result, a complex texture can exhibit a stronger overall attachment force than a simple texture of equivalent surface liberation. This textural advantage is particularly beneficial for coarse particle recovery in low-turbulence environments like the NovaCell™, where competing detachment forces are minimised. Consequently, the metallurgical advantage of the NovaCell™ over conventional technologies in recovering poorly liberated coarse particles is likely to be most pronounced when treating ores characterised by complex, disseminated locking textures. Bubbles of different diameters will also interact differently with different size attachment sites and different induction times may be needed to ensure drainage and rupture of the water film to

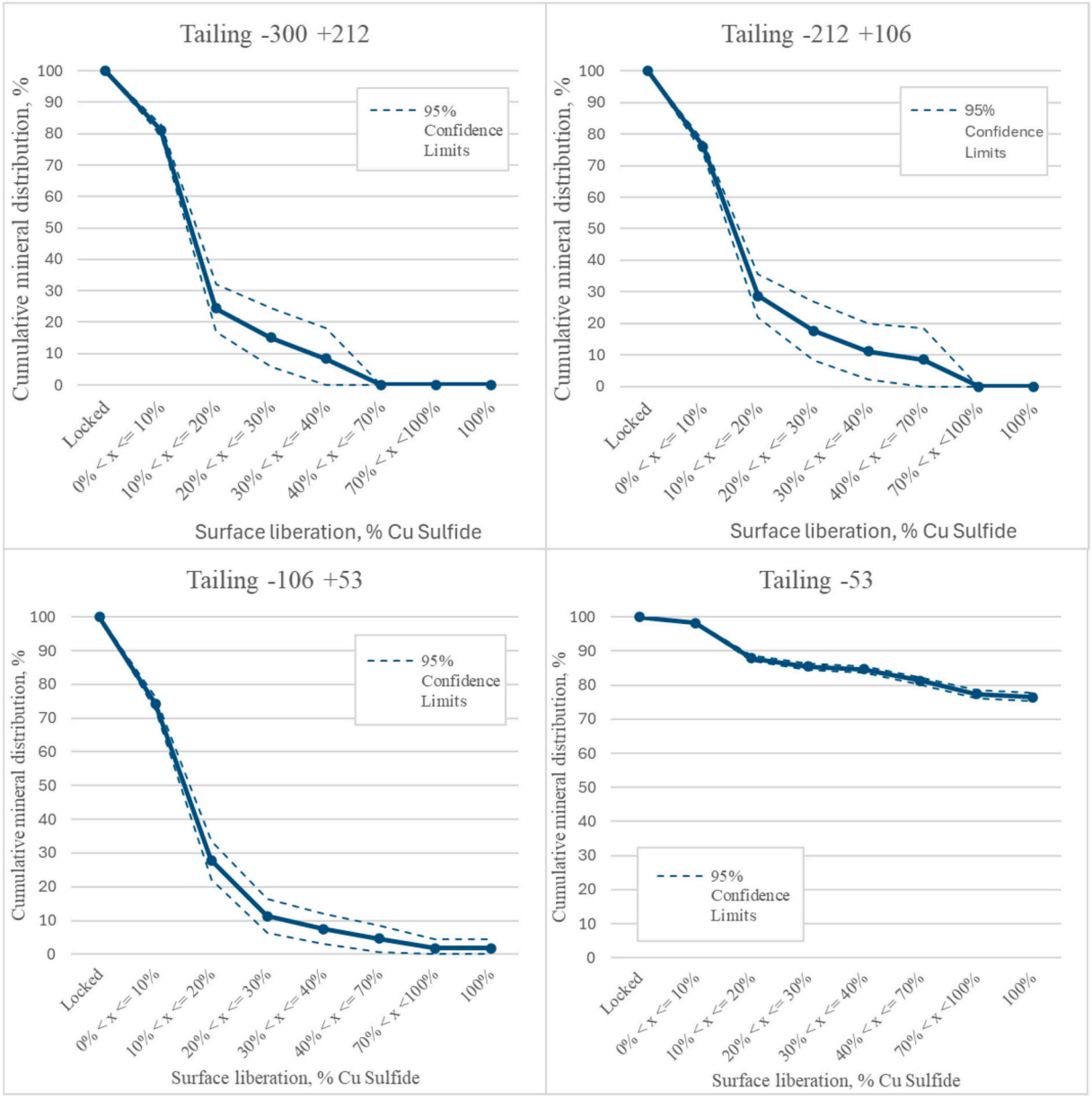

Fig. 17. Confidence limits of cumulative copper sulfide mineral distribution for each size fraction of the tailings sample.

allow attachment. The complex textured particle may also require multiple bubbles to attach to it to allow flotation. Where small bubbles attach to a coarse particle with only a few small attachment sites, the combined buoyant force of the formed multi-bubble single-particle aggregate may not be large enough to lift the particle. This can rob the site of the opportunity to attach to a larger bubble capable of floating the particle. Where multiple attachment sites are present, particles may become buoyant in the fluidized bed but not buoyant in the less dense supernatant pulp immediately above the bed interface. These particles may collide with positively buoyant aggregates rising out of the bed and form "clusters", where multiple bubbles and particles combine to form a large aggregate (Ata et al., 2009; Jameson et al., 2020). This assembly of both positively and negatively buoyant aggregates can result in a cluster with a net positive buoyancy, allowing the recovery of otherwise unrecoverable particles. This is further enhanced by the increased cross-sectional area of the cluster, allowing the upward flow in the Nova-Cell™ to cause a particle to rise even if it is neutrally or slightly negatively buoyant. Such described clusters are quite stable when exposed to mild agitation but easily torn apart when exposed to higher magnitude forces of mechanically agitated cells (Chen et al., 2015a,2015b).

The effect of different locking textures may be compounded by the specific mineral associations of each textural class. In the ore tested, complex locking textures were more highly associated with high density iron oxides, while the simple locking textures were more frequently observed in the relatively lower density silicate minerals. The higher particle density associated with complex locking textures increases their inertia, making them more susceptible to shear-induced detachment from bubbles within the turbulent flotation environment. Consequently, these particles are more prone to detachment when subjected to the turbulent hydrodynamic forces in the cell.

3.8. Flowsheet implications

If the grind size in a flotation circuit was to be increased in pursuit of operational, economic, and environmental benefits, it will be accompanied by a reduction in the surface liberation of composite particles. The inherent turbulence of conventional mechanical cells makes them largely unsuitable for recovering such particles, particularly those

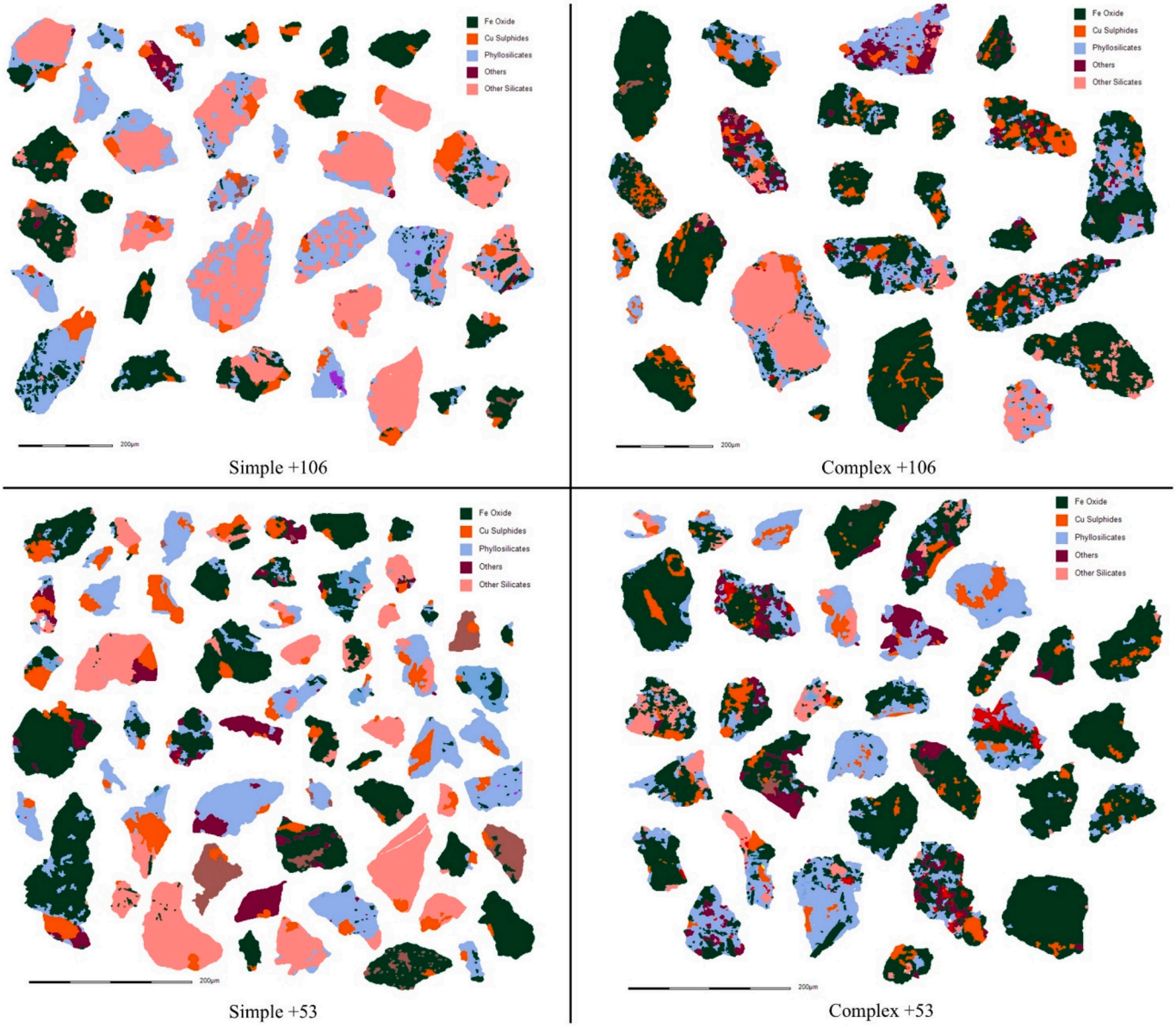

Fig. 18. False-colour images of particles with between 10 % and <100 % liberation found in the 212–106 µm and 106–53 µm size fractions of the tailings, separated by simple (left) and complex (right) locking textures.

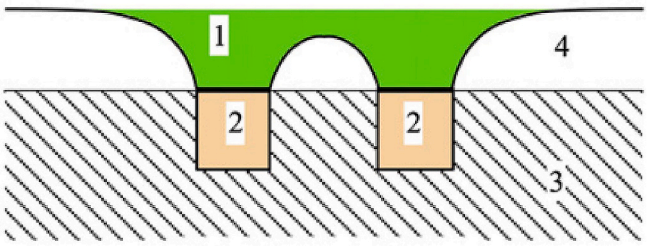

Fig. 19. Bridging gas–liquid interface on a composite surface with multiple close attachment sites. (1) Gas phase; (2) hydrophobic attachment site; (3) hydrophilic host mineral; (4) liquid phase (Gautam and Jameson, 2012).

exhibiting complex locking textures. Conversely, the quiescent hydrodynamic conditions of fluidized-bed technologies such as the NovaCell™ overcome these physical limitations by supporting the stability of delicate bubble-particle aggregates. The ability to successfully recover poorly liberated, coarse composites offers significant metallurgical and operational advantages within modern mineral processing flowsheets. When utilised in a pre-concentration duty, coarse particle flotation enables the early rejection of a coarse, barren tail, bypassing the energy-intensive comminution required in existing flowsheets to achieve high degrees of surface liberation. This early gangue rejection effectively upgrades the feed to downstream conventional circuits, which can lower economic cut-off grades and potentially extend mine life. Furthermore, integrating coarse particle flotation technology into rougher or scavenger applications permits a targeted increase in the primary grind size. Coarser primary grinding directly unlocks additional plant throughput and reduces specific energy consumption, while simultaneously generating coarser tailings that improve dewatering rates and simplify overall water recovery and tailings management. Additionally, because the NovaCell™ treats a broad feed size distribution including fines, it provides these benefits without the capital and operational complexity of dedicated upstream classification circuits. During continuous operation, the NovaCell™ simultaneously acts as a flotation machine and classification device, producing a bulk concentrate alongside distinct coarse

and fine tailings streams. This built-in classification offers significant flowsheet flexibility, allowing these sized tailings to be seamlessly routed to downstream technologies that are highly specialised for narrow size fractions.

3.9. Further work

Optimisation of process parameters for both technologies was not fully explored in this study.

For the mechanical cell, the standard operational approach of increasing overall residence time to improve bubble exposure would likely yield further increases in recovery. For the NovaCell™, optimising the internal recycle rate during continuous operation could similarly extend exposure time, while adjusting the energy dissipation rate within the downcomer could be used to directly improve the fundamental bubble-particle collision efficiency, as could adjusting the impeller design or rotational speed for the mechanical cell. Exploring these targeted parameter changes may allow for further reductions in the fine and ultra-fine particles lost to tailings. Another parameter not explored was the effect of increasing the collector type or collector dosage. The short chain xanthate collector used in this study could be replaced with a longer chain xanthate to increase the hydrophobicity of composite particles and strengthen the bubble-particle attachment force. It has been shown that increasing collector dosage can increase the attachment efficiency of partially liberated composites (Ralston et al., 2007). Additionally, fine and coarse particles typically require larger collector dosages when compared to intermediate particles (Boulton et al., 2003); fine particles require higher dosages because their large specific surface area demands more reagent for adequate coverage, while coarse particles require increased dosages to maximise hydrophobicity and strengthen bubble attachment against competing detachment forces. Further reagent optimisation may lead to improved recoveries of both fully liberated fines and poorly liberated coarse composites. Finally, optimisation of the pulp chemistry to synergise with the collector could yield improved results.

4. Conclusions

This study investigated the performance of the NovaCell™, a flotation machine featuring a quiescent fluidized bed, in recovering coarse and composite copper sulfide particles from a run-of-mine ore, benchmarked against a conventional mechanically agitated cell. A comprehensive analysis, combining flotation tests with detailed mineral liberation analysis (MLA) of the NovaCell™ products, was conducted to quantify the recovery response as a function of both particle size and surface liberation.

The results demonstrated the superior performance of the NovaCell™, which achieved an overall copper recovery of 94.3 % ± 0.8 % compared to 89.4 % ± 0.8 % in the mechanical cell. The performance advantage was most pronounced for coarse particles, with the NovaCell™ maintaining high copper recovery at particle sizes above 106 μm while there was a sharp decrease in recovery above this size for the mechanical cell. The subsequent liberation analysis of the NovaCell™ products provided a key insight into its mechanism of recovery. High copper recoveries were consistently achieved for all particle size fractions that exhibited a surface liberation of 10 % or greater. Given the inherent tendency for two-dimensional stereological analysis to overestimate true three-dimensional liberation values, it can be confidently concluded that the NovaCell™ is highly effective at recovering particles with as little as 10 % surface liberation, and potentially even lower. This capability is attributed to the quiescent hydrodynamic conditions within the fluidized bed, which minimise the detachment forces that typically limit the recovery of coarse, poorly liberated, and complex-textured composite particles in turbulent mechanical cells.

The demonstrated ability of the NovaCell™ to recover poorly liberated particles unlocks significant flowsheet benefits. By enabling flotation at a coarser grind size, it offers the potential for increased plant throughput, substantial reductions in energy consumption and associated emissions, and simplified water recovery and tailings management. This positions the technology as a valuable tool for various duties, including pre-concentration to upgrade feed to existing circuits or as a rougher/scavenger to directly enhance recovery in the primary circuit.

Furthermore, there is potential to enhance performance beyond what was observed in this study by optimising the NovaCell™ operating parameters and reagents scheme. The findings confirm that flotation technologies designed to minimise turbulence, such as the NovaCell™, provide a robust solution to the long-standing challenge of coarse particle flotation, paving the way for more efficient and sustainable mineral processing flowsheets.

CRediT authorship contribution statement

Lonn M. Cooper: Writing – original draft, Writing – review & editing, Conceptualization, Methodology, Investigation, Formal analysis, Visualization. **Graeme J. Jameson:** Writing – review & editing. **Sherwin Morgan:** Project administration, Funding acquisition.

Declaration of competing interest

The authors declare that they have no known competing financial interests or personal relationships that could have appeared to influence the work reported in this paper.

Data availability

Data will be made available on request.

References

Ahmed, M.M., 2010. Effect of comminution on particle shape and surface roughness and their relation to flotation process. Int. J. Miner. Process. 94, 180–191.

Anfruns, J.P., Kitchener, J.A., 1976. The absolute rate of capture of single particles by single bubbles. In: Flotation. AIME New York, p. 625.

Ata, S., 2012. Phenomena in the froth phase of flotation — a review. Int. J. Miner. Process. 102–103, 1–12. https://doi.org/10.1016/J.MINPRO.2011.09.008.

Ata, S., Chen, Z., Jameson, G.J., 2009. Improving the capture of coarse particles using bubble clusters. Preprint 9–83.

Batterham, R.J., 2013. Major trends in the mineral processing industry. BHM Berg- Hüttenmännische Monatshefte 158, 42–46. https://doi.org/10.1007/s00501-013-0109-0.

Boulton, A., Fornasiero, D., Ralston, J., 2003. Characterisation of sphalerite and pyrite flotation samples by XPS and ToF-SIMS. Int. J. Miner. Process. 70, 205–219. https://doi.org/10.1016/S0301-7516(03)00003-6.

Chen, Z., Ata, S., Jameson, G.J., 2015a. Breakup and re-formation of bubble clusters in a flotation cell. Miner. Eng. 71, 16–20.

Chen, Z., Ata, S., Jameson, G.J., 2015b. Behaviour of bubble clusters in a turbulent flotation cell. Powder Technol. 269, 337–344.

Gontijo, D.F., Fornasiero, C., Ralston, D., 2007. The limits of fine and coarse particle flotation. Can. J. Chem. Eng. 85, 739–747. https://doi.org/10.1002/cjce.5450850519.

Deming, W.E., 1938. Statistical adjustment of data. New York : Dover Publications.

Falutsu, M., Dobby, G.S., 1989. Direct measurement of froth drop back and collection zone recovery in a laboratory flotation column. Miner. Eng. 2, 377–386. https://doi.org/10.1016/0892-6875(89)90006-X.

Finch, J.A., Dobby, G.S., 1990. Column flotation. Flotat. Sci. Eng. 291–329.

Fosu, S., Awatey, B., Skinner, W., Zanin, M., 2015a. Flotation of coarse composite particles in mechanical cell vs. the fluidised-bed separator (the HydroFloat™). Miner. Eng. 77, 137–149. https://doi.org/10.1016/j.mineng.2015.03.011.

Fosu, S., Skinner, W., Zanin, M., 2015b. Detachment of coarse composite sphalerite particles from bubbles in flotation: Influence of xanthate collector type and concentration. Miner. Eng. 71, 73–84. https://doi.org/10.1016/j.mineng.2014.10.014.

Fuerstenau, M.C., Jameson, G.J., Yoon, R.-H., 2007. Froth flotation: a century of innovation. SME.

Gautam, A., Jameson, G.J., 2012. The capillary force between a bubble and a cubical particle. Miner. Eng. 36–38, 291–299. https://doi.org/10.1016/j.mineng.2012.05.018.

Jameson, G.J., 2012. The effect of surface liberation and particle size on flotation rate constants. Miner. Eng. 36–38, 132–137. https://doi.org/10.1016/j.mineng.2012.03.011.

Jameson, G.J., 2010. New directions in flotation machine design. Miner. Eng. 835–841. https://doi.org/10.1016/j.mineng.2010.04.001.

Jameson, G.J., Cooper, L., Tang, K.K., Emer, C., 2020. Flotation of coarse coal particles in a fluidized bed: the effect of clusters. Miner. Eng. 146. https://doi.org/10.1016/j.mineng.2019.106099.
Jameson, G.J., Emer, C., 2024. Effect of bubble loading on the recovery of coarse mineral particles by flotation. Miner. Eng. 215. https://doi.org/10.1016/j.mineng.2024.108788.
King, R.P., 1982. Principles of flotation South African Institute of Mining and Metallurgy. Kelvin House 2.
Koh, P.T.L., Hao, F.P., Smith, L.K., Chau, T.T., Bruckard, W.J., 2009. The effect of particle shape and hydrophobicity in flotation. Int. J. Miner. Process. 93, 128–134.
Kohmuench, J., Mankosa, M., Yan, E., Wyslouzil, H., Christodoulou, L., Luttrell, G., 2010. Advances in coarse particle recovery - fluidised-bed flotation. XXV International Mineral Processing Congress 2010.
Kohmuench, J.N., Luttrell, G.H., Mankosa, M.J., 2001. Coarse particle concentration using the HydroFloat separator. Min. Metall. Explor. 18, 61–67. https://doi.org/10.1007/BF03402873.
Leigh, G.M., Sutherland, D.N., Gottlieb, P., 1993. Confidence limits for liberation measurements. Miner. Eng.
Lotter, N.O., Baum, W., Reeves, S., Arrué, C., Bradshaw, D.J., 2018. The business value of best practice process mineralogy. Miner. Eng. 116, 226–238. https://doi.org/10.1016/j.mineng.2017.05.008.
Lotter, N.O., Whittaker, P.J., Kormos, L., Stickling, J.S., Wilkie, G.J., 2002. The development of process mineralogy at Falconbridge Limited and application to the Raglan Mill. CIM Bull. 95, 85–92.
Lynch, A.J., Johnson, N.W., Manlapig, E. V, Thorne, C.G., 1981. Mineral and coal flotation circuits: Their simulation and control.
Mehrfert, P.J., 2017. Investigating the potential of HydroFloat (TM) coarse particle flotation techniques on copper sulphide ores. In: 49th Annual Canadian Mineral Processors, Ottawa, pp. 17–19.
Miettinen, T., Ralston, J., Fornasiero, D., 2010. The limits of fine particle flotation. Miner. Eng. 23, 420–437. https://doi.org/10.1016/j.mineng.2009.12.006.
Miller, J.D., Lin, C.-L., Hupka, L., Al-Wakeel, M.I., 2009. Liberation-limited grade/recovery curves from X-ray micro CT analysis of feed material for the evaluation of separation efficiency. Int. J. Miner. Process. 93, 48–53. https://doi.org/10.1016/j.minpro.2009.05.009.
Morgan, S., Amelunxen, P., Akerstrom, B., Cooper, L., 2023. Pinto Valley Mine, Copper Recovery Study with the NovaCell TM. In: Proceedings MetPlant 2023, pp.101–115.
Morgan, S., Jameson, G.J., Cooper, L., 2024. NovaCell TM-Technology to Meet the World's Future Copper Demands, in: IMPC 2024-31st IMPC-International Mineral Processing Congress (pp. 2827–2839). SME.
Muganda, S., Zanin, M., Grano, S.R., 2011. Influence of particle size and contact angle on the flotation of chalcopyrite in a laboratory batch flotation cell. Int. J. Miner. Process. 98, 150–162. https://doi.org/10.1016/j.minpro.2010.11.004.
Ralston, J., Fornasiero, D., Grano, S., Duan, J., Akroyd, T., 2007. Reducing uncertainty in mineral flotation-flotation rate constant prediction for particles in an operating plant ore. Int. J. Miner. Process. 84, 89–98. https://doi.org/10.1016/j.minpro.2006.08.010.
Schulze, H.J., 1984. Physico-chemical elementary processes in flotation: an analysis from the point of view of colloid science including process engineering considerations / Hans Joachim Schulze ; [translated by Manfred Hecker]. Elsevier Amsterdam ; New York. Developments in mineral processing 4.
Schulze, H.J., 1977. New theoretical and experimental investigations on stability of bubble/particle aggregates in flotation: a theory on the upper particle size of floatability. Int. J. Miner. Process.
Seaman, B.A., Vollert, L., 2017. Recovery of coarse liberated gold particles using pneumatically assisted fluidized bed flotation. Proceedings of World Gold Conference.
Soto, H., Barbery, G., 1991. Flotation of coarse particles in a counter-current column cell. Min. Metall. Explor. 8, 16–21. https://doi.org/10.1007/BF03402925.
Trahar, W.J., 1981. A rational interpretation of the role of particle size in flotation. Int. J. Miner. Process. 8, 289–327.
Verrelli, D.I., Bruckard, W.J., Koh, P.T.L., Schwarz, M.P., Follink, B., 2014. Particle shape effects in flotation. Part 1: Microscale experimental observations. Miner. Eng. 58, 80–89.
Welsby, S.D.D., Vianna, S.M.S.M., Franzidis, J.-P., 2010. Assigning physical significance to floatability components. Int. J. Miner. Process. 97, 59–67. https://doi.org/10.1016/j.minpro.2010.08.002.
Wiegel, R.L., 2006. The rationale behind the development of one model describing the size reduction/liberation of ores. 2006 SME Annual Conference - Advances in Comminution 2006, 225–241.
Wightman, E.M., Evans, C.L., 2014. Representing and interpreting the liberation spectrum in a processing context. Miner. Eng. 61, 121–125. https://doi.org/10.1016/j.mineng.2013.12.012.
Wotruba, H., Hoberg, H., Schneider, F.U., 1991. Investigation on the separation of microlithe and zircon. The influence of particle shape on floatability. In: Preprints. XVII. International Mineral Processing Congress, pp. 23–28.
Yekeler, M., Ulusoy, U., Hiçyılmaz, C., 2004. Effect of particle shape and roughness of talc mineral ground by different mills on the wettability and floatability. Powder Technol. 140, 68–78.